ChemComm

COMMUNICATION

View Article Online
View Journal | View Issue

Cite this: *Chem. Commun.*, 2021, 57, 9296

Received 18th June 2021,
Accepted 18th August 2021

DOI: 10.1039/d1cc03235f

rsc.li/chemcomm

Liquid metal assisted sonocatalytic degradation of organic azo dyes to solid carbon particles†

Olawale Oloye,[ab] James D. Riches [bc] and Anthony P. O'Mullane [*ab]

Room temperature liquid metals are an emerging class of materials for a variety of heterogeneous catalytic reactions. In this work we explore the use of Ga based liquid metals as a sonochemical catalyst for the degradation of organic azo dyes such as methyl orange, congo red and eriochrome black T. Rapid degradation to non toxic solid carbon particles was achieved over a large dye concentration range to produce differently sized particles *via* both bath and probe sonication which could be repeated multiple times with the same catalyst.

Tremendous effort has been channelled recently towards the exploration of post-transition liquid metal alloys including Field's metal, Rose's metal, Wood's metal and non-toxic room-temperature gallium-based liquid metals due to their relatively low-melting-point and distinctive physical and chemical properties.[1] In particular liquid Ga has attracted increasing attention in the field of actuators, gas sensors, fuel cells, biomedical applications, electromechanical systems, and catalysis.[2] A key aspect for catalysis is the preparation of micro/nanosized droplets *via* ultrasonication to increase the surface area available for reaction. The majority of studies have focused on using sonication to produce monodisperse particle/droplet size either by changing the method of sonication, *i.e.* bath sonicator *versus* probe sonicator, introducing capping agents to prevent agglomeration or changing the solvent and its temperature in which the particles/droplets are dispersed.[3] However little attention has been paid towards investigating chemical reactions that may be accessible during sonication. Given the reactive environment created during sonication which induces cavitation and localised regions of high temperature and pressure it presents an opportunity to investigate the degradation of harmful pollutants using liquid metals as potential sonocatalysts.

Organic pollutant degradation is of interest because the continuous discharge of industrial dye effluents into terrestrial bodies has altered the ecosystem.[4] The textile industry widely uses azo synthetic dyes, and their waste disposal poses both environmental and socio-economic challenges.[4a,5] These pigments are known to be non-biodegradable, xenobiotic, toxic and carcinogenic, causing adverse environmental and health problems.[4a,6] Azo dyes are recalcitrant to conventional aerobic (biological) processes, and commonly used physical/chemical treatment methods are often neither cost-effective nor eco-friendly,[6a,7] producing toxic by-products.[8]

Ultrasonication has been used to degrade organic species in solution in the presence of metallic or semiconducting particles that can induce the formation of reactive oxygen species such as hydroxide/superoxide radicals that can degrade organic molecules.[9] Examples include zero valent iron that utilises the Fenton process to generate hydroxide radicals,[10] or ZnO nanomaterials under both illumination and sonication.[11] However degradation in the dark is required as illuminating reactors at scale is problematic. Examples of sonochemical dye degradation in the dark are Fe-doped TiO_2 nanoparticles,[12] or Pd nanoparticles immobilised on carbon nanodots[13] which showed discolouration of the solution but no analysis of the by-products. For industrial wastewater treatment the complete destruction of organic species is preferred, yet the long term and immediate toxic impact of dye degradation products on living organisms are not fully understood.[4a] Herein, we investigated the degradation of a series of azo dyes *via* ultrasonication in the presence of liquid metal Galinstan (GaInSn) and Ga under dark conditions which ultimately creates solid carbonaceous deposits.

The process is simple whereby a liquid metal drop is immersed into a vial containing the dye solution and sonicated either in a bath or *via* a probe sonicator. Upon sonication the

[a] *School of Chemistry and Physics, Queensland University of Technology (QUT), Brisbane, QLD 4001, Australia. E-mail: anthony.omullane@qut.edu.au*
[b] *Centre for Materials Science, Queensland University of Technology (QUT), Brisbane, QLD 4001, Australia*
[c] *Central Analytical Research Facility (CARF), Queensland University of Technology (QUT), Brisbane, QLD 4001, Australia*

† Electronic supplementary information (ESI) available: Structures of dyes, digital images of degraded solutions, XRD of used catalyst, SEM of carbon particles. See DOI: 10.1039/d1cc03235f

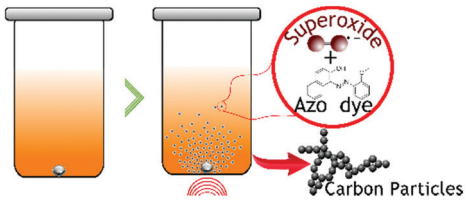

Scheme 1 Simplified representation of the degradation of azo-dye to carbon particles.

liquid metal disperses into micro/nanodroplets which has been extensively reported in aqueous solution.[3a,c,d,14] A diagram illustrating the process is shown in Scheme 1. In this work a series of water-soluble azo dyes, characterised by a central N═N bond, were investigated including methyl orange (MO), congo red (CR) and eriochrome black T (EB), the chemical structures of which are illustrated in Fig. S1 (ESI†). The initial liquid metal used in this work was Galinstan (68.5% Ga, 21.5% In and 10.0% Sn) due to the wide temperature range at which it is liquid.

Fig. 1 shows a digital image of the initial 12.4 mg L^{-1} solution of MO, as well as a typical solution after 1 h bath sonication in the presence of the liquid metal when the solution was allowed to settle for removal of the liquid metal droplets. This data shows the effectiveness of the process to discolour the solution and as discussed later to degrade the dye to form carbonaceous products. The MO system was then investigated in detail and is discussed here. During optimisation of the process, it was found that sonicating MO in deionised water made the recovery of galinstan more involved and required centrifugation to remove all the droplets. Therefore, the solution was acidified to prevent extensive surface oxide formation on the liquid metal droplets. This enabled the liquid metal droplets to coalesce into a large liquid metal droplet that was easy to remove from solution and allowed the process to be repeated. To ensure the process could be followed by UV-vis spectroscopy the concentration of dye used was 12.4 mg L^{-1} and is shown in Fig. 1b. A large absorbance peak at 464 nm with a smaller peak at 272 nm are due to MO as seen for the initial solution ($S1_i$). These peaks shift to slightly longer wavelength (of 481 nm and 276 nm) when the solution is acidified ($S2_i$) which is typical for this dye. After the first sonication cycle these peaks completely disappear for both for the MO/deionised H_2O solution ($S1_f$) and the acidified solution ($S2_f$) where the latter showed a degradation efficiency of 99%. Due to the ease of recovery of the liquid metal in the acidified solution, further cycles were undertaken and it can be seen from the UV-vis spectra (Fig. 1b) that high degradation efficiency was maintained of up to 98% for 4 runs. The effect of sonication time was then investigated where it was found that complete degradation occurred after 30 min. To further reduce the time a probe sonicator was used where degradation occurred after 10 min (Fig. 1c). The catalyst was then analysed after multiple runs and the XRD pattern did indicate that some GaOOH had formed during the course of the reaction (Fig. S2, ESI†) but was still active for dye degradation when re-used.

Previous work has shown that degradation of MO occurs *via* cleavage of the N═N bond which results in decolourisation leading to the formation of other organic species in solution such as *N*,*N*-dimethyl-*p*-phenylenediamine (DMPD) and 4-aminobenzenesulfonate (structures are shown in Fig. S3, ESI†).[15] To check for such degradation products, FTIR and high performance liquid chromatography (HPLC) were performed. The FTIR spectrum of an evaporated solution (Fig. 2a) is largely featureless and does not show any evidence of MO. HPLC of the solution was then undertaken and the chromatogram (Fig. 2b) does not show evidence of MO but one peak occurs at a 5 min retention time. Further analysis with LC-MS (Fig. S4, ESI†) indicated some 4-aminobenzenesulfonate formed and explains the peak at 254 nm in Fig. 1b.

To understand the catalytic mechanism, scavenging experiments were carried out as it is established that sonication results in the formation of radical species that can degrade organic molecules. Ethanol, ethylenediaminetetraacetic acid (EDTA) and *p*-benzoquinone (BQ) were used as scavengers to probe the formation of hydroxyl radicals ($^{\bullet}OH$), holes (h^+) and superoxide radicals ($O_2^{\bullet -}$), respectively.[13] The only major decrease observed in sonocatalytic activity was with 1,4 benzoquinone, which indicates that superoxide radicals are the main reactive species (Fig. 2c). The creation of these radicals would result in cleavage of the azo linkage (–N═N–) and therefore decolorization occurs as shown by the UV-vis spectra.

This method was also tested for other azo dyes including congo red and eriochrome black T where the UV-vis spectra of the solutions before and after sonication are shown in Fig. 3a and b, respectively. The data shows the complete degradation of the dye under the same conditions, *i.e.* a slightly acidic

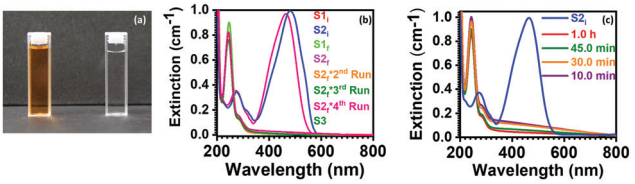

Fig. 1 (a) Digital images of (i) 12.4 mg L^{-1} MO and (ii) representative image of the supernatant obtained after sonication degradation, (b) UV-Vis spectra of 12.4 mg L^{-1} MO ($S1_i$), 12.4 mg L^{-1} MO in acidic solution ($S2_i$) and after liquid metal sonication degradation ($S2_f$) for runs 1–4 and (c) UV-vis spectra recorded as a function of sonication time and type of sonication (probe sonication – purple line).

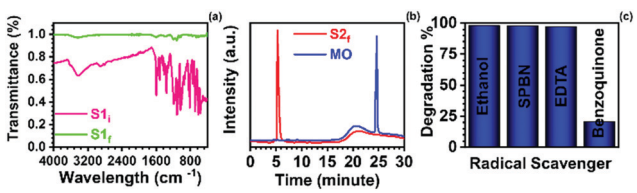

Fig. 2 (a) FTIR analysis of MO ($S1_i$) and dried supernatant ($S1_f$) after sonication, (b) HPLC analysis of MO and final supernatant solution ($S2_f$) and (c) plot demonstrating the influence of scavengers on the sonocatalytic degradation percentage for MO.

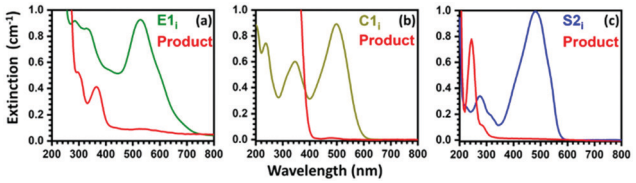

Fig. 3 UV-vis spectra of (a) eriochrome black T, (b) congo red before and after sonication with liquid metal galinstan and (c) UV-vis spectrum of MO before and after sonication with liquid Ga.

solution sonicated for 30 min. The liquid metal was also changed to Ga only and the temperature increased slightly to 30 °C so that Ga was liquid to begin with before sonication. This also resulted in rapid dye degradation (Fig. 3c and Fig. S5, ESI†) with a similar performance to liquid Galinstan and therefore the mechanism is not dependent on the presence of In and Sn in the liquid metal.

However, with time it was noticed that some black particles precipitated to the bottom of the reaction vial. Raman spectroscopy (Fig. 4b) was carried out which shows two peaks at 1322 and 1568 cm^{-1} indicating the presence of carbon which correspond to the D and G bands, respectively. The I_D/I_G ratio was determined to be 0.61 (Table S1, ESI†) which indicates that the material has some graphitic character. The sample was examined by FTIR spectroscopy (Fig. 4c) where the bands in the range of ~945 cm^{-1} and 1013 cm^{-1} are related to C–O stretching vibrations, and in the range of ~1121 cm^{-1} and 1166 cm^{-1} are related to C–O epoxy deformation and stretching vibration of sp^2 hybridized carbon atoms (C=C), respectively.[16] The bands at ~1518 cm^{-1} and 1604 cm^{-1} originate from the COOH and C=O edge functional groups. The presence of weak bands at ~2804 cm^{-1}, 2912 cm^{-1}, and 3230 cm^{-1} are ascribed to the stretching vibrations of O=C=O and C–H modes.[16a,c] Therefore, when considering the Raman and FTIR data it indicates that there is a significant amount of carbon present in the black deposit which contain oxygen functional groups on the surface. XPS spectra of the material are shown in Fig. 4a. The C 1s core level spectrum shows contributions at 284.6, 285.7 and 287.7 eV, which corresponds to C–C, C–O–C and O–C=O groups respectively, which is consistent with the FTIR data and previous reports of carbon nanomaterials.[17a–c] The O 1s spectrum shows contributions at 531.3 eV and 534.5 eV, corresponding to C–O–C and O=C–OH groups, respectively.[18] XPS analysis showed that nitrogen was present in the sample with a main peak at 399.4 eV and a minor shoulder at 403.0 eV, corresponding to C–N–C and N–$(C)_3$ groups respectively.[17a] The Ga 2p spectrum indicated a trace amount of Ga in the samples. To confirm whether the samples are potentially doped with nitrogen, they were etched with an ion beam and the subsequent XPS spectra are shown in Fig. S6 (ESI†) show little change indicating that some nitrogen incorporation has likely occurred.

The above analyses were undertaken with an initial dye concentration of 12.4 mg L^{-1}. The concentration was then increased to 100 mg L^{-1} to probe how effective this approach is for organic molecule degradation. It was found that this sonication approach with liquid metal is highly effective resulting in complete discolouration of the MO, CR and EB dyes after 1 h of bath sonication (Fig. S7, ESI†). Significantly this also resulted in the extensive formation of carbon which was confirmed by SEM/EDX analysis of the deposit after reaction (Fig. 5a).

It was found that clusters of carbon particles of the order of 200 nm were formed in addition to some Ga particles (Fig. 5a). The oxygen map showed that the most concentrated regions were associated with the Ga particles as expected given the reactivity of Ga with oxygen to form oxides. The particles agglomerate together into clusters as seen in the SEM image while AFM indicated particle heights up to 10 nm (Fig. S8a, ESI†). TEM images in Fig. 5b show some individual amorphous carbon particles where there is a homogeneous distribution of C and O in the particles. A lower magnification SEM image shows the large extent of carbon particle formation in these samples (Fig. S8b, ESI†). At the lowest MO concentration (12.4 mg L^{-1}) carbon nanoparticles of *ca.* 10 nm diameter were formed as seen by TEM imaging (Fig. S9, ESI†). This indicates that the particle size is dependent on the initial dye concentration, increasing from 10 to 200 nm at the higher dye concentration.

For the mechanism it is postulated that the initial step is formation of superoxide radicals which attack the N=N bond resulting in decolourisation of the solution. These radicals are

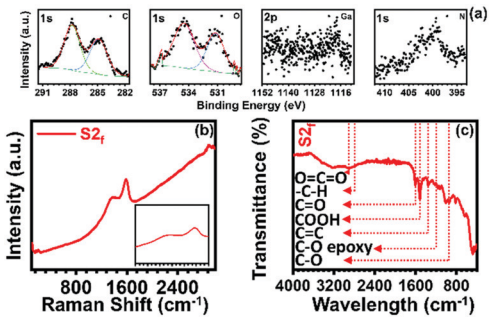

Fig. 4 XPS core level spectra for C, O, Ga, and N (a), Raman spectrum (b), FTIR spectrum (c) of the sample $S2_f$.

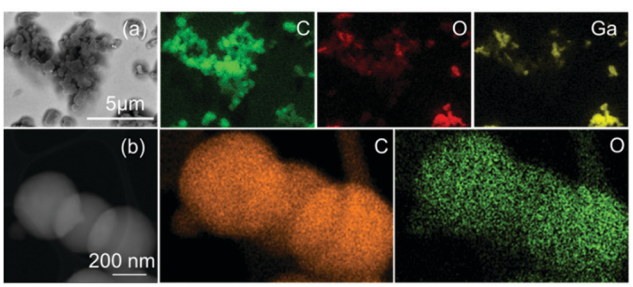

Fig. 5 (a) SEM image and EDX analysis showing agglomerated carbon particles obtained from degradation of 100 mg L^{-1} MO, (b) TEM image and EDX analysis of the carbon particles.

formed due to the presence of some semiconducting GaOOH (Fig. S2, ESI†) which has a CB edge position of −0.87 V *vs.* NHE which is lower than the $O_2/O_2^{-\bullet}$ couple at −0.33 V, therefore dissolved O_2 is reduced when electrons are excited into the CB. Under sonochemical conditions with metal particles in solution, a heterogeneous system is setup which differs significantly to a homogeneous system. Here liquid metal micro/nanodroplets will continuously form in solution creating many heterogeneous liquid metal/aqueous dye interfaces as well as high velocity inter particle collisions. This is reflected in the time dependent bath sonication study (Fig. S10, ESI†) which shows that there is an induction time for the first 10 min (where the liquid metal is dispersed) after which degradation occurs rapidly over the next 5 min and then slows. This was confirmed using a pre dispersed catalyst which showed that degradation could then be achieved with the bath sonicator in only 10 min (Fig. S11, ESI†). It has been reported that the effective transient temperature reached at the point of impact during inter-particle collisions can be as high as 3000 °C.[19] Under such extreme conditions organic molecules produced after superoxide radical attack will break down resulting in the formation of solid carbon species. Also, Ga metal has been used as a catalyst in C–C bond coupling reactions which may also play a role in forming solid carbon products.[20] This could be a key factor as previous work which investigated sonochemical dye degradation using Pd nanoparticles immobilised on carbon dots only resulted in decolourisation and not carbon formation.[13]

In summary, we have successfully demonstrated the sonocatalytic degradation of a series of organic azo dyes with an efficiency of 99% where the liquid metal catalyst was reusable. The ease of reusability/recovery of the catalyst is attributed to use of a slightly acidic media which inhibits extensive formation of gallium oxide and allows the liquid metal droplets to coalesce. The major reactive species was identified as superoxide radicals which attacks the dye during sonication, however formation of solid carbon was observed due to the highly reactive environment of colliding liquid metal droplets. This approach could potentially be extended to a range of other organic species that are harmful to the environment.

AOM acknowledges funding from the Australian Research Council (DP170102138). Authors acknowledge the instrumentation, technical support of the QUT Central Analytical Research Facility (CARF).

Conflicts of interest

There are no conflicts to declare.

Notes and references

1 (*a*) S. Idrus-Saidi, J. Tang, M. B. Ghasemian, J. Yang, J. Han, N. Syed, T. Daeneke, R. Abbasi, P. Koshy, A. P. O'Mullane and K. Kalantar-Zadeh, *J. Mater. Chem. A*, 2019, 7, 17876–17887; (*b*) Y. Liu, W. Zhang and H. Wang, *Mater. Horiz.*, 2021, **8**, 56–77; (*c*) K. Zuraiqi, A. Zavabeti, F.-M. Allioux, J. Tang, C. Nguyen, P. Tafazolymotie, M. Mayyas, A. Ramarao, M. Spencer, K. Shah, C. F. McConville, K. Kalantar-Zadeh, K. Chiang and T. Daeneke, *Joule*, 2020, **4**, 2290–2321; (*d*) H. Song, T. Kim, S. Kang, H. Jin, K. Lee and H. J. Yoon, *Small*, 2020, **16**, 1903391; (*e*) S. Chen, H.-Z. Wang, R.-Q. Zhao, W. Rao and J. Liu, *Matter*, 2020, **2**, 1446–1480; (*f*) S.-Y. Tang, D. R. Mitchell, Q. Zhao, D. Yuan, G. Yun, Y. Zhang, R. Qiao, Y. Lin, M. D. Dickey and W. Li, *Matter*, 2019, **1**, 192–204; (*g*) K. Kalantar-Zadeh, J. Tang, T. Daeneke, A. P. O'Mullane, L. A. Stewart, J. Liu, C. Majidi, R. S. Ruoff, P. S. Weiss and M. D. Dickey, *ACS Nano*, 2019, **13**, 7388–7395; (*h*) T. Daeneke, K. Khoshmanesh, N. Mahmood, I. de Castro, D. Esrafilzadeh, S. J. Barrow, M. D. Dickey and K. Kalantar-zadeh, *Chem. Soc. Rev.*, 2018, **47**, 4073–4111.

2 (*a*) O. Oloye, C. Tang, A. Du, G. Will and A. P. O'Mullane, *Nanoscale*, 2019, **11**, 9705–9715; (*b*) M. D. Dickey, *ACS Appl. Mater. Interfaces*, 2014, **6**, 18369–18379; (*c*) S. Y. Tang, Y. Lin, I. D. Joshipura, K. Khoshmanesh and M. D. Dickey, *Lab Chip*, 2015, **15**, 3905–3911; (*d*) M. Shafiei, F. Hoshyargar, N. Motta and A. P. O'Mullane, *Mater. Des.*, 2017, **122**, 288–295; (*e*) S.-Y. Tang, V. Sivan, P. Petersen, W. Zhang, P. D. Morrison, K. Kalantar-zadeh, A. Mitchell and K. Khoshmanesh, *Adv. Funct. Mater.*, 2014, **24**, 5851–5858; (*f*) J. Crawford, M. A. Sayeed and A. P. O'Mullane, *Colloids Surf., A*, 2021, **623**, 126750.

3 (*a*) J. N. Hohman, M. Kim, G. A. Wadsworth, H. R. Bednar, J. Jiang, M. A. LeThai and P. S. Weiss, *Nano Lett.*, 2011, **11**, 5104–5110; (*b*) S. Idrus-Saidi, J. Tang, J. Yang, J. Han, T. Daeneke, A. P. O'Mullane and K. Kalantar-Zadeh, *ACS Sens.*, 2020, **5**, 1177–1189; (*c*) Y. Lin, J. Genzer, W. Li, R. Qiao, M. D. Dickey and S.-Y. Tang, *Nanoscale*, 2018, **10**, 19871–19878; (*d*) Y. Lin, Y. Liu, J. Genzer and M. D. Dickey, *Chem. Sci.*, 2017, **8**, 3832–3837.

4 (*a*) D. Rawat, V. Mishra and R. S. Sharma, *Chemosphere*, 2016, **155**, 591–605; (*b*) A. Bafana, S. S. Devi and T. Chakrabarti, *Environ. Rev.*, 2011, **19**, 350–371.

5 C. Wang, J. Jin, Y. Sun, J. Yao, G. Zhao and Y. Liu, *Chem. Eng. J.*, 2017, **327**, 774–782.

6 (*a*) A. Bafana, S. S. Devi and T. Chakrabarti, *Environ. Rev.*, 2011, **19**, 350–370; (*b*) O. Oloye, J. F. S. Fernando, E. R. Waclawik, D. Golberg and A. P. O'Mullane, *New J. Chem.*, 2020, **44**, 14979–14988.

7 C. Fernández, M. S. Larrechi and M. P. Callao, *Trends Anal. Chem.*, 2010, **29**, 1202–1211.

8 (*a*) H. Ben Mansour, Y. Ayed-Ajmi, R. Mosrati, D. Corroler, K. Ghedira, D. Barillier and L. Chekir-Ghedira, *Environ. Sci. Pollut. Res.*, 2010, **17**, 1371–1378; (*b*) E. Choudhary, N. Capalash and P. Sharma, *J. Environ. Pathol., Toxicol. Oncol.*, 2004, **23**, 279–285.

9 Z. Wu, A. Abramova, R. Nikonov and G. Cravotto, *Ultrason. Sonochem.*, 2020, **68**, 105195.

10 B. Chen, X. Wang, C. Wang, W. Jiang and S. Li, *Ultrason. Sonochem.*, 2011, **18**, 1091–1096.

11 C. Lops, A. Ancona, K. Di Cesare, B. Dumontel, N. Garino, G. Canavese, S. Hérnandez and V. Cauda, *Appl. Catal., B*, 2019, **243**, 629–640.

12 Z. Ait-Touchente, A. M. Khalil, S. Simsek, S. Boufi, L. F. V. Ferreira, M. Rei Vilar, R. Touzani and M. M. Chehimi, *Cellulose*, 2020, **27**, 1085–1097.

13 A. Selim, S. Kaur, A. H. Dar, S. Sartaliya and G. Jayamurugan, *ACS Omega*, 2020, **5**, 22603–22613.

14 W. Zhang, J. Z. Ou, S.-Y. Tang, V. Sivan, D. D. Yao, K. Latham, K. Khoshmanesh, A. Mitchell, A. P. O'Mullane and K. Kalantar-zadeh, *Adv. Funct. Mater.*, 2014, **24**, 3799–3807.

15 Y. Sha, I. Mathew, Q. Cui, M. Clay, F. Gao, X. J. Zhang and Z. Gu, *Chemosphere*, 2016, **144**, 1530–1535.

16 (*a*) G. Rajender and P. K. Giri, *J. Mater. Chem. C*, 2016, **4**, 10852–10865; (*b*) Y. Sun, S. Wang, C. Li, P. Luo, L. Tao, Y. Wei and G. Shi, *Phys. Chem. Chem. Phys.*, 2013, **15**, 9907–9913; (*c*) R. K. Biroju, G. Rajender and P. K. Giri, *Carbon*, 2015, **95**, 228–238.

17 (*a*) M. Zhao, *Appl. Sci.*, 2018, **8**, 1303; (*b*) S. J. Bradley, R. Kroon, G. Laufersky, M. Röding, R. V. Goreham, T. Gschneidtner, K. Schroeder, K. Moth-Poulsen, M. Andersson and T. Nann, *Microchim. Acta*, 2017, **184**, 871–878; (*c*) Y. Li, S. Li, Y. Wang, J. Wang, H. Liu, X. Liu, L. Wang, X. Liu, W. Xue and N. Ma, *Phys. Chem. Chem. Phys.*, 2017, **19**, 11631–11638.

18 G. Hong, H. Zhao, H. Deng, H. Yang, H. Peng, Y. Liu and W. Chen, *Int. J. Nanomed.*, 2018, **13**, 4807–4815.

19 K. S. Suslick, *Science*, 1990, **247**, 1439–1445.

20 B. Qin and U. Schneider, *J. Am. Chem. Soc.*, 2016, **138**, 13119–13122.